CORE
Metadata, citation and similar papers at core.ac.uk
Provided by DigitalCommons@CalPoly

AGU PUBLICATIONS

JGR

Journal of Geophysical Research: Oceans

RESEARCH ARTICLE

10.1002/2014JC009998

Key Points:
- Regional upwelling and relaxation cycles modulate offshore stratification
- Changes in offshore stratification modify the nearshore internal bore field
- Upwelling regimes and bores are important for assessing oxygen variability

Correspondence to:
R. K. Walter,
rwalter@stanford.edu

Citation:
Walter, R. K., C. B. Woodson, P. R. Leary, and S. G. Monismith (2014), Connecting wind-driven upwelling and offshore stratification to nearshore internal bores and oxygen variability, *J. Geophys. Res. Oceans*, *119*, 3517–3534, doi:10.1002/2014JC009998.

Received 25 MAR 2014
Accepted 19 MAY 2014
Accepted article online 22 MAY 2014
Published online 6 JUN 2014

Connecting wind-driven upwelling and offshore stratification to nearshore internal bores and oxygen variability

Ryan K. Walter[1], C. Brock Woodson[2], Paul R. Leary[3], and Stephen G. Monismith[1]

[1]Environmental Fluid Mechanics Laboratory, Stanford University, Stanford, California, USA, [2]COBIA Lab, College of Engineering, University of Georgia, Athens, Georgia, USA, [3]Hopkins Marine Station, Stanford University, Pacific Grove, California, USA

Abstract This study utilizes field observations in southern Monterey Bay, CA, to examine how regional-scale upwelling and changing offshore (shelf) conditions influence nearshore internal bores. We show that the low-frequency wind forcing (e.g., upwelling/relaxation time scales) modifies the offshore stratification and thermocline depth. This in turn alters the strength and structure of observed internal bores in the nearshore. An internal bore strength index is defined using the high-pass filtered potential energy density anomaly in the nearshore. During weak upwelling favorable conditions and wind relaxations, the offshore thermocline deepens. In this case, both the amplitude of the offshore internal tide and the strength of the nearshore internal bores increase. In contrast, during strong upwelling conditions, the offshore thermocline shoals toward the surface, resulting in a decrease in the offshore internal tide amplitude. As a result, cold water accumulates in the nearshore (nearshore pooling), and the internal bore strength index decreases. Empirical orthogonal functions are utilized to support the claim that the bore events contribute to the majority of the variance in cross-shelf exchange and transport in the nearshore. Observed individual bores can drive shock-like drops in dissolved oxygen (DO) with rapid onset times, while extended upwelling periods with reduced bore activity produce longer duration, low DO events.

1. Introduction

The nearshore coastal ocean, defined here as the innermost portion of the continental shelf and extending from the shoreline up to several kilometers offshore, is generally taken to be one of the most productive and ecologically important parts of the ocean [*Pauly and Christensen*, 1995; *Mann*, 2000]. The nearshore is also a complex environment from a physical standpoint, due in large part to the widespread and often irregular occurrence of nonlinear internal waves (NLIWs) that frequently appear more bore-like than wave-like [e.g., *Scotti and Pineda*, 2004; *Leichter et al.*, 1996; *Nam and Send*, 2011; *Davis and Monismith*, 2011; *Walter et al.*, 2012]. Indeed, this region of the ocean can be thought of as the "swash zone" for larger-scale internal wavefields on the continental shelf. These nearshore NLIWs have considerable implications for the cross-shelf exchange and transport of nutrients, sediments, contaminants, larvae, and other scalars [*Wolanski and Pickard*, 1983; *Pineda*, 1991, 1994, 1995, 1999; *Leichter et al.*, 1996; *Boehm et al.*, 2002; *Noble et al.*, 2009]; turbulent mixing and dissipation [*Sandstrom and Elliot*, 1984; *Venayagamoorthy and Fringer*, 2007; *Nam and Send*, 2011; *Davis and Monismith*, 2011; *Walter et al.*, 2012]; and hypoxia development [*Booth et al.*, 2012]. Despite a growing body of literature on the subject [cf. *Leichter et al.*, 1996; *Klymak and Moum*, 2003; *Lerczak et al.*, 2003; *Scotti and Pineda*, 2004; *Shroyer et al.*, 2008; *Nam and Send*, 2011; *Davis and Monismith*, 2011; *Woodson et al.*, 2011; *Walter et al.*, 2012; *Wong et al.*, 2012], many questions still remain with respect to the evolution, fate, and impact of NLIWs in the nearshore environment and their connection to the larger-scale internal wave/tide field on the shelf.

Internal waves on the continental shelf are well studied in numerical, experimental, and theoretical fluid mechanics (see *Lamb* [2013] and the sources therein for a comprehensive review). Yet, the majority of the aforementioned numerical and laboratory studies [see *Lamb*, 2013] have necessarily focused on simplified, idealized setups, and isolated processes. Likewise, field studies have concentrated mainly on deeper shelf waters (50+ m depths) [cf. *Alford et al.*, 2012, Table 1], while the ultimate fate of NLIWs in the shallower, nearshore regions (~20 m) has been mainly speculative. The lifecycle and ultimate fate of internal waves propagating from the shelf to the nearshore environment is highly variable due to a dynamic environment with changing bathymetry, spatially and temporally evolving stratification, tidal and wind forcing, and

© 2014. American Geophysical Union. All Rights Reserved.

coastal upwelling/downwelling influences [*Pineda and Lopez*, 2002; *Davis and Monismith*, 2011; *Lamb*, 2013]. Thus, further field observations are needed to assess the influence of changing environmental conditions on the offshore to onshore (shelf to nearshore) translation of internal wave/tide fields in the coastal environment.

Nearshore internal bores are a common feature that produce transient stratification and mixing events, and represent the dominant source of variability, in the ecologically important region of southern Monterey Bay, CA [*Walter et al*., 2012]. Internal bores in this region are characterized by an upslope surging flow of dense water that tends to stratify the water column ("bore period" from *Walter et al*. [2012]). The bore period is followed by a strongly sheared downslope flow in the form of a warm-front, and high-frequency temperature oscillations, as the bore feature relaxes back downslope and returns the water column back to nearly its original state ("mixing period" from *Walter et al*. [2012]). During the mixing period, shear instabilities result in elevated levels of turbulent dissipation and diapycnal mixing in the stratified interior, consequently affecting local mixing dynamics that are critical for many ecologically important processes. Furthermore, the structure of the bores and relaxations in this region [see *Walter et al*., 2012] was examined with a numerical model and explained by the steep bathymetric slope in the region and dependence on the internal Iribarren number,

$$\xi = \frac{s}{\left(\frac{a}{\lambda}\right)^{1/2}}, \tag{1}$$

where s is the bathymetric slope, and a and λ are the offshore amplitude and wavelength of the incoming internal wave, respectively [e.g., *Boegman et al*., 2005]. While the bore characteristics were hypothesized to be dependent on regional-scale upwelling/downwelling and offshore conditions, that study focused on local dynamics of the observed internal bores in the nearshore [*Walter et al*., 2012].

The main objective of this study is to assess how wind forcing and offshore stratification influence nearshore internal bores, which are a common feature along many continental margins [*Shea and Broenkow*, 1982; *Holloway*, 1987; *Pineda*, 1991, 1994, 1995, 1999; *Pineda and Lopez*, 2002; *Leichter et al*., 1996; *Colosi et al*., 2001; *Klymak and Moum*, 2003; *Hosegood and van Haren*, 2004; *Nam and Send*, 2011]. For instance, in the Southern California Bight, *Pineda and Lopez* [2002] hypothesized that the observed nearshore internal bores were dependent on low-frequency wind forcing (e.g., upwelling/relaxation time scales) through the modification of the offshore stratification and thermocline depth. We test this hypothesis in southern Monterey Bay, a region strongly influenced by regional-scale upwelling/downwelling [e.g., *Rosenfeld et al*., 1994].

Additionally, we examine how offshore conditions and nearshore internal bores affect nearshore dissolved oxygen (DO) variability and the potential development of hypoxia, which has drawn significant attention in recent years [*Chan et al*., 2008; *Hofmann et al*., 2011]. While oxygen minimum zones (OMZs) occur naturally [*Wyrtki*, 1962; *Kamykowski and Zentara*, 1990; *Helly and Levin*, 2004], climatic changes appear to have driven OMZ expansions [*Keeling and Garcia*, 2002; *Stramma et al*., 2008, 2010] and brought OMZs into shallower shelf margins [*Bakun*, 1990; *Grantham et al*., 2004; *Helly and Levin*, 2004; *Bograd et al*., 2008]. The increased prevalence of inner shelf hypoxic intrusions has caused massive mortalities, and other deleterious impacts, to fish and invertebrates [*Grantham et al*., 2004; *Ekau et al*., 2010; *McClatchie et al*., 2010]. Upwelling-driven hypoxic events occur primarily via direct advection of low DO, subthermocline waters [*Grantham et al*., 2004; *Bograd et al*., 2008; *Chan et al*., 2008]. Internal bores are another DO transport mechanism and act to drive intrusions of hypoxic water at higher frequencies than low-frequency upwelling/relaxation cycles [*Booth et al*., 2012]. We show that these two DO transport processes, upwelling/relaxation cycles and internal bores, are not independent. Furthermore, we expand on the *Booth et al*. [2012] study and link regional upwelling dynamics and nearshore internal bore activity to the strength and frequency of low DO events, and DO variability, in the nearshore.

In section 2, we introduce the field site, the experimental setup, and data processing methods. Section 3 describes the high-resolution observations made over a 3 week study period and connects the regional-scale upwelling/relaxation trends with the offshore conditions and stratification. This is followed by results that link the offshore characteristics with the nearshore internal bores. Section 4 qualifies the findings over the 3 week study period using lower-resolution measurements made over an 2.5 month time period.

© 2014. American Geophysical Union. All Rights Reserved.

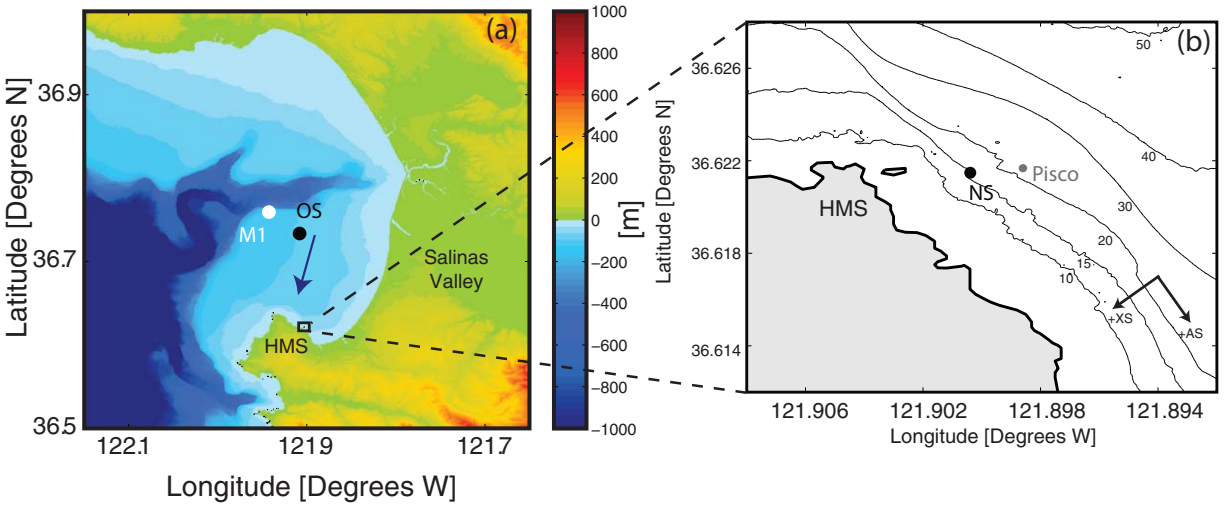

Figure 1. (a) Bathymetry and topography of the Monterey Bay, CA region with the study site indicated by a black box. The filled circles represent the offshore mooring (OS, black) and M1 buoy (white). Also shown is the median bore propagation heading from *Walter et al*. [2012] (blue arrow). (b) Study site with the nearshore mooring (NS) shown as a filled black circle. Bathymetry contours (10, 15, 20, 30, 40, and 50 m isobaths) shown along with the location of Hopkins Marine Station (HMS—Stanford University).

Section 4 also discusses biological and ecological implications of the results and highlights the interconnectedness of the shelf and the nearshore. Specifically, the potential for cross-shelf transport, as well as oxygen variability and low oxygen events, are discussed since internal bores are an important mechanism by which deeper offshore waters are transported to the nearshore. Finally, we summarize the findings in section 5.

2. Site Description and Methods

2.1. Study Site

Monterey Bay, located along the eastern Pacific Ocean and central California coast, is a semienclosed embayment that contains one of the largest submarine canyons in the United States (Figure 1a). Covering an area of 550 km^2, the bay features a narrow shelf (i.e., shelf break of 100 m within a few kilometers from the coast at some locations) with about 80% of the bay shallower than 100 m [*Breaker and Broenkow*, 1994]. Monterey Bay harbors an extremely large ecological diversity including some of the west coast's largest kelp (*Macrocystis pyrifera*) forests, marine reserve systems, large commercial fisheries, and eco-tourism industries [*Kildow and Colgan*, 2005; *Raheem et al*., 2011].

General physical conditions in Monterey Bay include tides that are mixed semidiurnal, with currents dominated by the M_2 (12.42 h period) tidal component (M_2 tidal amplitude of 0.5 m) [see *Rosenfeld et al*., 2009; *Carter*, 2010]. Currents on the shelf tend to be 180° out of phase relative to the canyon (i.e., directed out of the bay on the flood tide due to inflow through the canyon) [*Petruncio et al*., 1998; *Carter*, 2010]. Large amplitude internal waves are a ubiquitous and well-documented phenomenon along the continental margin in and around the Monterey Submarine Canyon, where isopycnal displacements often reach hundreds of meters [e.g., *Breaker and Broenkow*, 1994; *Petruncio et al*., 1998; *Kunze et al*., 2002]. Additionally, numerical models have confirmed both the local generation of internal tides, as well as the interaction of locally and remotely generated internal tides, at the M_2 tidal period inside the canyon and near the shelf edge [*Carter*, 2010; *Kang and Fringer*, 2012]. Finally, as mentioned earlier, internal motions in the form of bores are a common feature in the nearshore regions of southern Monterey Bay, and based on their observed propagation direction, seem to originate near the canyon mouth (Figure 1a) [*Walter et al*., 2012].

During the upwelling season in Monterey Bay (April to September), regional upwelling favorable winds (northwesterly) create a strong upwelling jet at Point Año Nuevo that flows southward across the mouth of the bay [*Rosenfeld et al*., 1994]. During periods of strong upwelling favorable winds (typically lasting 5–14 days), dense upwelled waters inundate the shelf and begin to accumulate, as the main offshore thermocline rises toward the surface. This process is interrupted during regional wind relaxation events lasting several days, whereby upwelling favorable winds weaken [cf. *Beardsley et al*., 1987].

© 2014. American Geophysical Union. All Rights Reserved.

2.2. Experimental Setup

The current study was part of a larger project (Monterey Tower Node—MOTOWN) aimed at understanding how nearshore internal bores affect circulation dynamics and turbulent mixing in the nearshore coastal environment. Here we focus on connecting regional-scale dynamics and upwelling to observed nearshore internal bores. Turbulent mixing by the nearshore bores, as well as various budgets (e.g., energy, momentum, etc.), will be investigated in future contributions. As such, only the moored instrument arrays and data used in this study will be described here.

Several densely instrumented moorings were deployed from 3 to 24 August 2012 (3 weeks) in southern Monterey Bay, CA. The nearshore mooring (NS; Figure 1b) was deployed on the 15 m isobath just offshore of Hopkins Marine Station (HMS—Stanford University, Pacific Grove, CA). This is the location of previous observations of nearshore internal bores [*Walter et al*., 2012], as well as regular intrusions of low DO water by internal motions [*Booth et al*., 2012]. In order to capture the vertical structure and high-frequency motions of the bores, this mooring was equipped with 22 SBE56 temperature loggers throughout the water column (0–9 m above the bed (mab) in 0.5 m increments, 10, 11, 12 mab), all of which were sampling at 0.5 s periods. NS also contained a SBE39 temperature logger at the surface, which sampled at 10 s intervals. Additionally, the mooring included SBE37 conductivity-temperature-depth (CTD) loggers at 0 (24 s), 2 (6 s), 4 (6 s), 6 (6 s), and 8 (24 s) mab, where the sampling interval is given in parentheses for each instrument. The NS site also had a SeapHOx at 1 mab measuring DO concentrations [e.g., *Frieder et al*., 2012]. An RDI 1200 kHz Workhorse acoustic Doppler current profiler (ADCP) was deployed at the NS site sampling in fast-ping Mode 12 (6 subpings per 1 s ensemble) with 0.5 m vertical bin spacing. This sampling scheme results in a small error standard deviation of 0.12 cm/s for 10 min averages, which is the averaging interval used in further analysis. The ADCP was also leveled by divers to within 1° of the horizontal using a bubble level in order to minimize instrument tilt errors.

In addition to the high-resolution measurements over the 3 week study period described above, long-term measurements from the same location over an 2.5 month study period (13 June to 31 August) were analyzed. Long-term measurements were from a near-bottom (1 mab) SBE56 temperature logger (2 s sampling period) and a SeapHOx measuring DO concentrations (10 min sampling period).

In order to capture regional-scale stratification and the upwelling-induced effect on the shelf, observations from an offshore mooring (OS; Figure 1a) on the shelf near the 85 m isobath were used. The OS mooring location also lines up with the previously observed propagation pathway (i.e., from near the canyon mouth to the NS site) of the nearshore internal bores (Figure 1b) [*Walter et al*., 2012]. This mooring was equipped with a vertical collection (1.75, 10, 20, 30, 40, 50, 60, 70 mab, and surface) of RBR TR-1040 temperature loggers sampling at 30 s intervals. During the experiment, the near-surface thermistor malfunctioned and so the surface temperature was obtained at 30 min intervals using the nearby National Data Buoy Center (NDBC) buoy 46092 (M1; Figure 1a). The offshore mooring also had CTDs located at 3 and 70 mab, sampling at 30 s and 3 min intervals, respectively. The OS mooring collected data over the 2.5 month period (13 June to 31 August). Results from the 3 week period (3–24 August) are presented in conjunction with the high-resolution NS measurements in section 3, while the long-term results (2.5 month period) are discussed in section 4.

Regional, offshore winds were collected at 10 min intervals from the NDBC buoy 46042 (36.785°N, 122.469°W). All times referenced in the text and figures are in local time, Pacific Daylight Time, unless otherwise noted.

2.3. Analyses

Velocity measurements from the NS ADCP were rotated into cross-shore, along-shore, and vertical velocity components using the principal axes obtained from a long-term ADCP near the site (Figure 1b; PISCO—Partnership for Interdisciplinary Studies of Coastal Oceans). The principal axes of the long-term record were within 2° of those calculated in the current study. Regional, upwelling favorable winds were calculated using the mean along-coast direction across Monterey Bay (north-northwesterly winds from 330°) [e.g., *Woodson et al*., 2009].

During the summer upwelling season, salinity variations in Monterey Bay are sufficiently small so that density is largely controlled by temperature [e.g., *Woodson et al*., 2009, 2011; *Walter et al*., 2012]. Analysis of the nearshore CTD data showed that small changes in salinity varied linearly with temperature throughout the

© 2014. American Geophysical Union. All Rights Reserved.

water column (e.g., $R^2 = 0.91$, p value < 0.001 for the 2 mab CTD) with nearly identical linear regression coefficients between different depths. Therefore, densities at all nearshore thermistor locations were calculated using the observed temperature and derived linear relationship from the CTD measurements for salinity as a function of temperature. Density profiles at the offshore site were calculated using the same method described above with the offshore CTD data ($R^2 = 0.58$, p value < 0.001 for the temperature-salinity regression using 10 min averages of both the 3 and 70 mab CTDs). The lower coefficient of determination in the OS regression versus the NS regression is likely the result of large regional relaxations that act to advect open ocean water masses with marginally lower salinities into the Bay. These water masses deviate slightly from the general temperature-salinity relationship; however, the salinity deviations are small and do not contribute significantly to the density calculation.

Spectral and coherence calculations were performed using the fast Fourier transform (FFT), following standard methods [e.g., *Walter et al*., 2011]. Hamming windows with 50% overlap between adjacent segments were used with the choice of window length in the calculations representing a compromise between the number of degrees of freedom (DOF) for confidence intervals, frequency resolution, and length of the original record. Confidence intervals for the spectra were calculated using a chi-square variable analysis and the equivalent number of DOF (EDOF). For the coherence analysis, confidence limits were quantified using the EDOF [*Emery and Thompson*, 2004].

A dynamical analysis of the bores requires an index that can accurately quantify their strength and intensity. This index also needs to be robust enough to capture the non-canonical and shock-like nature of the bores. Whereas conventional internal wave analysis considers perturbations to a well-defined and quasi steady background density field, often defined as the low-pass filtered density field [e.g., *Nash et al*., 2005], the bore features observed at this site do not follow this convention. Specifically, the bores often propagate into a well-mixed (i.e., unstratified) water column in the nearshore, making the conventional internal wave approach invalid since there is no well-defined "background state," and the highly nonlinear, asymmetric bores do not behave in a wave-like manner. Rather, the bores are characterized by nonlinear pulses of dense fluid in and out of the nearshore, similar to an estuarine flow where dense water from the ocean advects up and down the estuary during the tidal cycle. The conventional approach in the current study leads to a bore hysteresis effect, whereby the background state is contaminated by the previous bore events. This illustrates the need for a more robust proxy for the observed features that accounts for their bore-like properties (i.e., nonlinear, asymmetric, and transient) and the observed background conditions.

Based on the above considerations, we define a bore strength proxy using the potential energy density anomaly often used in estuarine flows [*Simpson et al*., 1978],

$$\phi = -\frac{g}{H}\int_0^H (\rho - \rho_m) z dz, \tag{2}$$

where g is the gravitational acceleration, H is the water column depth, z is the height above the bottom, and $\rho_m = \frac{1}{H}\int_0^H \rho dz$ is the depth mean density. The potential energy density anomaly represents the amount of energy required to mix the water column completely, and hence is an index of stratification. Since the instantaneous vertical distribution over depth is used, the proxy accurately captures the transient stratification and mixing events associated with the bores. In order to delineate bores during the nearshore periods when stratification is present, as well as the periods when the bores propagate into a well-mixed environment, the bore strength index is defined as the high-pass filtered (33 h half-amplitude period) potential energy density anomaly. Results were not sensitive to the filter period used.

The effect of the temporally varying, regional stratification on the offshore internal wave/tide field is examined using a linear, normal mode analysis. This theory considers normal mode perturbations to a stratified fluid, and in the longwave limit, leads to the following linear eigenvalue problem:

$$\begin{aligned} \frac{d^2\hat{\psi}}{dz^2} + \frac{N^2}{c^2}\hat{\psi} &= 0, \\ \hat{\psi}(0) &= 0, \\ \hat{\psi}(H) &= 0, \end{aligned} \tag{3}$$

© 2014. American Geophysical Union. All Rights Reserved.

where $N^2(z) = -\frac{g}{\rho_o}\frac{\partial \overline{\rho}}{\partial z}$ is the buoyancy frequency squared, $\overline{\rho}$ is a time-averaged density profile, and $\hat{\psi}$ and c are eigenfunction and eigenvalue pairs corresponding to the vertical structure function and phase speed of a linear disturbance, respectively. The largest eigenvalue, and the focus of this study, corresponds to the linear, longwave speed (c_{lw}). We use the phase speed as a proxy for the strength of the offshore stratification, and consequently the offshore internal wave/tide field. Thus, changes in the offshore (regional) internal wave/tide field will be examined using the time variability of c_{lw}.

3. Results

3.1. General Observations

The time series of regional upwelling favorable winds measured during the study clearly shows multiple periods (7–10 days) of prolonged upwelling winds interspersed with relaxation events (2–3 days) where the winds diminish (Figure 2a). During upwelling episodes, the offshore temperature structure is highlighted by cooling throughout the water column, especially near the bottom (Figure 2b). This facet is consistent with advection of cooler waters from the deep, offshore environment. Correspondingly, the offshore thermocline shoals toward the surface, while the near-surface stratification decreases, as evident in the expansion of the highlighted isotherms (Figure 2b). In contrast, during weak upwelling favorable conditions or regional relaxation occurrences, the offshore temperature field warms, and the thermocline deepens (Figure 2b). During these periods, near-surface stratification also increases, as seen in the compression of the isotherms and increase in the vertical temperature gradient (Figure 2b). Likewise, vertical fluctuations in the thermocline increase in magnitude during the relaxations, in comparison to the upwelling periods (Figure 2b). From henceforth, the offshore thermocline depth will refer to the distance from the sea surface to the vertical location of the 11.2°C isotherm. Besides capturing the vertical gradients in the offshore stratification and the offshore internal wave activity well, this particular isotherm was chosen to delineate the thermocline since it is an isotherm that regularly appears with internal bores in the nearshore. However, all statistics and conclusions presented hereafter are valid for other isotherms within the thermocline region (e.g., 12.4°, 12.15°, 11.5°, 11.2°, etc.).

The nearshore site is marked by repeated pulses of cold water intrusions (i.e., nearshore internal bores) that advect in and out of the nearshore environment (Figure 2c). During weak upwelling favorable conditions and/or relaxations when the offshore thermocline is deep, the internal bore features propagate along the bed into well-mixed waters in the nearshore. These bores are characterized by transient stratification (upslope flow) and mixing (downslope flow) events, whereby the water column nearly returns to its original, well-mixed state following the downslope flow. In many cases, the bore events perturb and stratify the entire water column. The structure of the bore events during weak upwelling/relaxation conditions is consistent with previous observations made during the early upwelling season by *Walter et al*. [2012]. During extended periods of upwelling favorable conditions when the offshore thermocline becomes shallower, the structure is quite different. Rather than propagating into well-mixed waters near the bottom of the water column, the bores perturb a preexisting stratification along the nearshore thermocline (Figure 2c). This preexisting stratification is the result of the extended upwelling conditions, whereby cool, offshore waters inundate the nearshore and begin to accumulate, or "pool" (Figure 2c). From hereafter, we will refer to this process as nearshore pooling.

The arrival of an internal bore is characterized by a strong near-bottom onshore (upslope) flow in the cross-shore and an along-shore flow out of the bay (Figures 2e and 2f). During the relaxation of the bore (i.e., advecting out of the nearshore), the cross-shore velocity is highlighted by strong offshore (downslope) flow, while the along-shore velocity is directed back into the bay (Figures 2d and 2e) [see *Walter et al*., 2012].

Examination of the NS potential energy density anomaly over the record reveals large fluctuations during weak upwelling conditions and relatively weaker fluctuations during the upwelling periods and nearshore pooling (Figure 3a). These fluctuations are superposed on a low-frequency trend, whereby during active upwelling the low-pass signal increases due to the increased stratification (i.e., nearshore pooling, Figure 3a). Removing this low-frequency trend yields the high-passed anomaly, or the bore strength proxy. The bore strength proxy characterizes the magnitude of the nearshore internal bores and closely follows the scale of the perturbation to the nearshore temperature field (Figures 3b and 2c, respectively). During

© 2014. American Geophysical Union. All Rights Reserved.

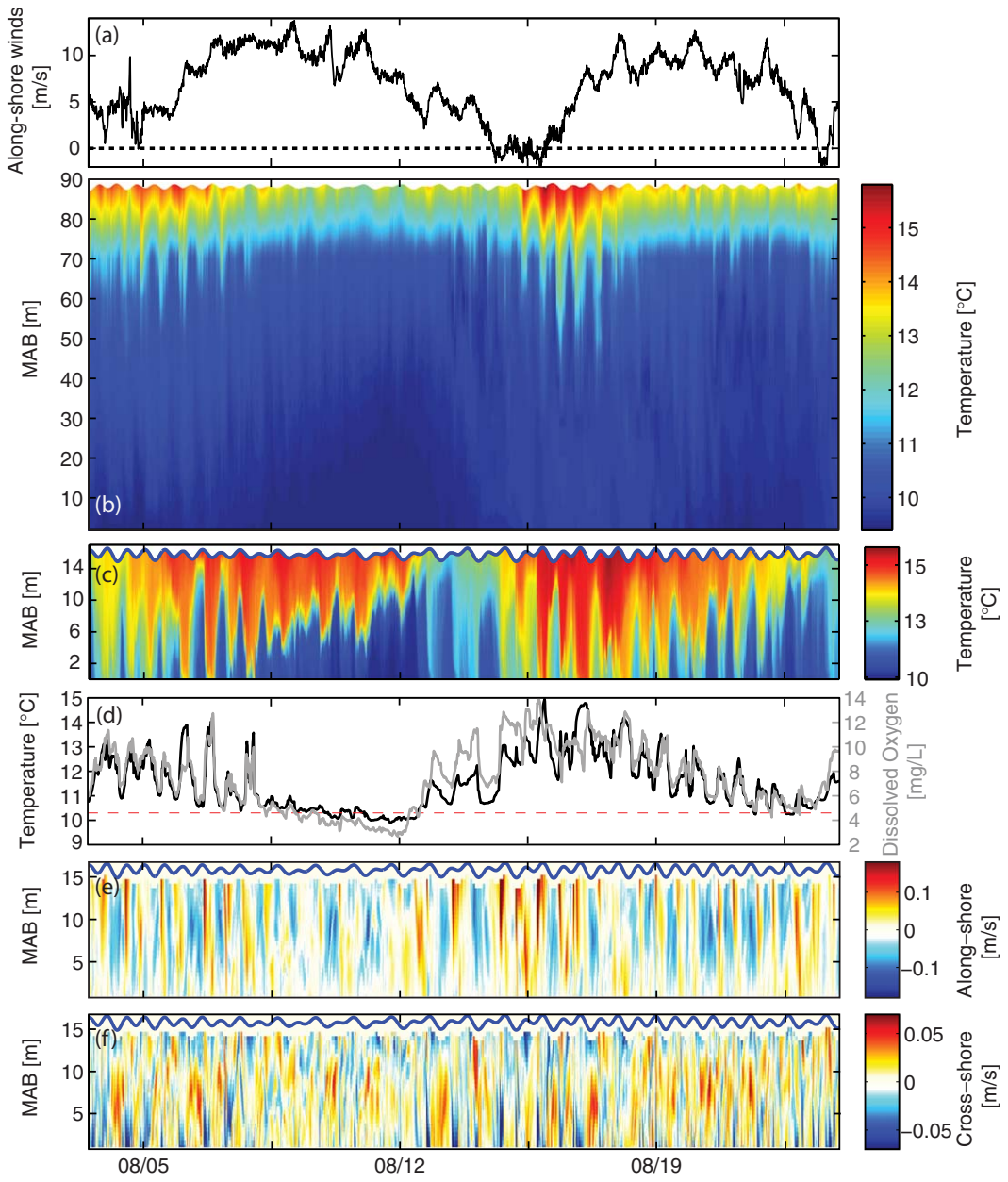

Figure 2. Time series over the 3 week study period of the (a) regional upwelling favorable winds (positive), (b) vertical temperature structure at the offshore (OS) mooring (11.2°C and 12.15°C isotherms shown as solid black lines highlight the thermocline structure), (c) vertical temperature structure at the nearshore (NS) mooring, (d) near-bottom temperature (left axis, black) and dissolved oxygen (right axis, gray) at the NS mooring, and the vertical velocity structure (10 min averages) at the NS mooring for the (e) along-shore (positive into the bay) and (f) cross-shore (positive onshore) velocity components, respectively. The location of the sea surface (blue line) is shown in Figures 2b, 2c, 2e, and 2f. The dashed red line in Figure 2d denotes the DO concentration identified by *Vaquer-Sunyer and Duarte* [2008] as a critical biological threshold (i.e., below 4.6 mg/L; hypoxic).

weaker upwelling conditions, the bore index has the greatest magnitude (Figure 3b), and these large fluctuations align with the large amplitude bores that perturb nearly the entire water column. In contrast, during strong upwelling, the bore strength proxy is weak (Figure 3b). This aspect coincides with periods of nearshore pooling, during which the bores generate small-amplitude perturbations to the preexisting thermocline.

A time series of near-bed (1 mab) DO and temperature is shown in Figure 2d. Also highlighted is the DO concentration identified by *Vaquer-Sunyer and Duarte* [2008] as the threshold necessary to maintain 90% biodiversity (i.e., below 4.6 mg/L DO, 60% air saturation, hypoxic). Figure 2d highlights the strong

© 2014. American Geophysical Union. All Rights Reserved.

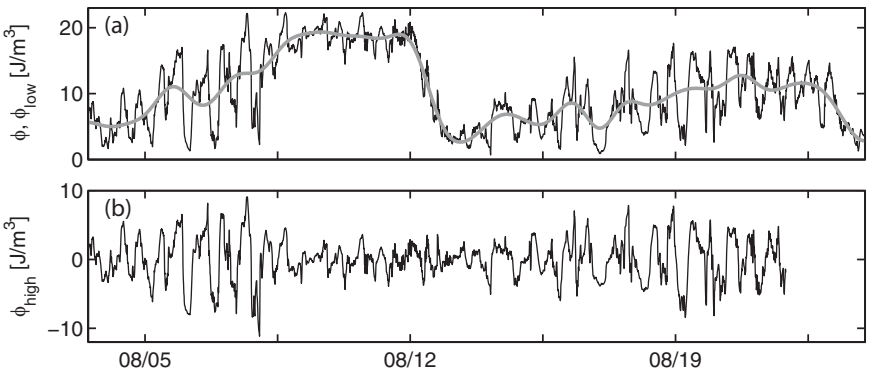

Figure 3. Time series over the 3 week study period of the (a) potential energy density anomaly (low-pass filtered time series shown in gray) and (b) high-pass filtered anomaly (bore strength proxy) at the nearshore (NS) study site.

covariation between DO concentration and water temperature (a linear regression between the two variables yields $R^2 = 0.77$, p-value < 0.001). During weak upwelling conditions and/or relaxations there are large fluctuations in DO and temperature, consistent with the large amplitude internal bores observed (e.g., Figure 3b). Likewise, the DO concentrations stay above the critical biological threshold, and low DO levels observed in individual bore events do not persist. This is likely due to a combination of both the advection of the low DO water back offshore, and the stronger vertical mixing observed during the warm-front relaxations of the bores that acts to reoxygenate the water column ("mixing period" from *Walter et al*. [2012]). In contrast, during upwelling favorable conditions, low DO levels persist for extended periods of time and the intense fluctuations of DO and temperature are not observed (Figure 2d). During the nearshore pooling period, the low DO levels persist below the 4.6 mg/L hypoxic level [*Vaquer-Sunyer and Duarte*, 2008] for nearly 3 days (9–12 August; Figure 2d) and reach as low as 2.66 mg/L. It is important to note that the DO measurements presented in Figure 2d are near-bed (1 mab) measurements, while the bores observed during upwelling conditions typically perturb the midwater thermocline region in the nearshore. Nonetheless, the decrease in DO fluctuations is consistent with the reduction in the bore strength index (Figure 3b).

Spectral analysis of the bore strength proxy reveals a dominant peak at the semidiurnal frequency (M_2 tidal component, Figure 4c). The offshore thermocline depth also shows a dominant peak near the M_2 tidal component; however, there is also significant energy at low frequencies (<0.3 cpd, Figure 4b). This low-frequency energy is consistent with the 7–10 days period of the offshore thermocline depth (Figure 2b). Regional upwelling favorable winds are dominated by lower frequencies (<0.3 cpd), while the semidiurnal variability is largely absent (Figure 4a).

3.2. Connecting Offshore and Nearshore Dynamics

Regional upwelling favorable winds are significantly coherent with the offshore thermocline depth at low frequencies (e.g., <0.4 cpd, Figure 5a). Analysis of the phase lag reveals that the thermocline height lags the winds at low frequencies of 0.3 and 0.1 cpd by 0.67 to 1.1 days, respectively (Figure 5b). The low-frequency coherence suggests that, as expected, the offshore stratification is largely governed by wind-driven upwelling/relaxation cycles during this 3 week period.

In order to examine how the temporally varying, offshore stratification affects the offshore internal wave/tide field, linear longwave speeds were calculated using a normal mode analysis (see section 2.3). The phase speed can be used as an index for the strength of the offshore stratification and internal waves. Figure 6 highlights how the phase speed changes over time due to the evolving offshore stratification. In particular, during periods of active upwelling when the offshore thermocline shoals toward the surface, phase speeds are lowest (i.e., wave amplitudes are the smallest). In contrast, during relaxation events, where surface waters are warmer and the thermocline is deeper, increased stratification leads to larger phase speeds. Active upwelling causes the thermocline to shoal toward the surface and decreases internal wave amplitudes, while relaxations deepen the thermocline and allow for increased wave phase speeds and amplitudes. Correspondingly, when the offshore wavefield is weakest during upwelling periods, the nearshore bore index (high-pass filtered potential energy density anomaly) also displays the smallest magnitudes

© 2014. American Geophysical Union. All Rights Reserved.

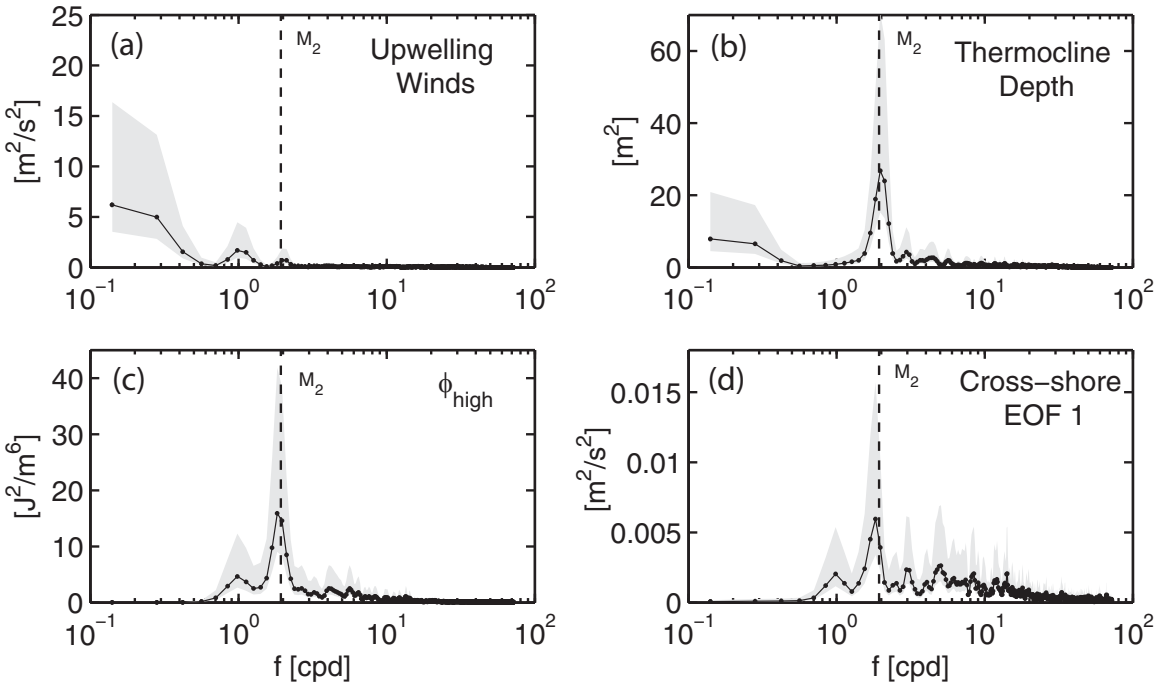

Figure 4. Variance-preserving power spectra over the 3 week study period of the (a) regional upwelling winds, (b) offshore thermocline depth (11.2°C isotherm), (c) high-pass filtered potential energy density anomaly (bore strength proxy), and (d) 1st mode, EOF amplitude time series of the cross-shore velocity field. 80% confidence intervals are denoted by gray shading and the location of the M_2 tidal component by a dashed black line.

(Figures 6 and 3b, respectively). Likewise, weak upwelling events/relaxations are highlighted by a stronger offshore internal wavefield that coincides with a larger nearshore bore index.

Coherence between the nearshore bore index and the offshore thermocline depth further supports the connection between offshore and nearshore internal dynamics. The two parameters are significantly coherent at the semidiurnal frequency ($\sim M_2$ tidal component, Figure 7a). Analysis of the phase lag indicates that the nearshore index lags the offshore thermocline height by ~2.0 h at this frequency (Figure 7b). Given that there are only two moorings in the current study, it is impossible to assess accurately the propagation speed and direction of the internal wavefield. Moreover, estimating internal wave transit times from the coherence analysis assumes that the internal wavefield is propagating on a direct line from the OS to the NS mooring, an assumption that cannot be validated in the current study.

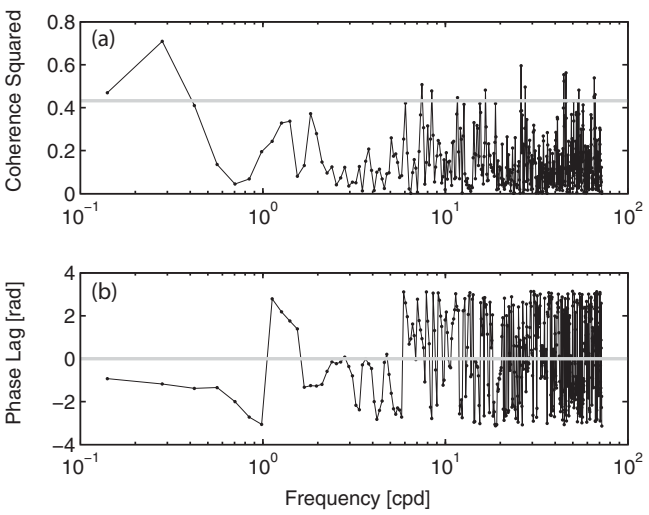

Figure 5. (a) Coherence squared and (b) phase lag between the regional upwelling favorable winds and the offshore thermocline depth (11.2°C isotherm) over the 3 week study period. The 95% confidence level is shown as a gray line in Figure 5a. A negative phase lag at a given frequency indicates that the upwelling winds lead the offshore thermocline depth.

4. Discussion

4.1. Long-Term Record and Offshore to Nearshore Connection

It is important to qualify the results presented above over the 3 week time period, especially since this short record only captured a few upwelling/relaxation cycles. To

© 2014. American Geophysical Union. All Rights Reserved.

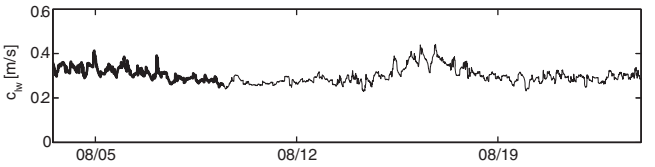

Figure 6. Linear, longwave phase speeds from the offshore mooring (black line) over the 3 week study period. Internal wave phase speeds were calculated using the offshore stratification (10 min averages) and a normal mode analysis (section 2.3). The gray shading denotes the phase speed in the presence of a typical barotropic current on the shelf of ±0.2 m/s [e.g., *Breaker and Broenkow*, 1994].

address this issue, we analyzed the OS data and low-resolution NS data (i.e., temperature and DO at 1 mab) that are available over an 2.5 month period (see section 2.2 for details). Figure 8a highlights that over the longer record the upwelling favorable winds are characterized by the same periodic upwelling/relaxation cycles at low frequencies (7–10 days) seen during the 3 week record [cf. *Beardsley et al*., 1987]. This periodicity is confirmed by the upwelling wind spectrum (Figure 9a), which also reveals the diurnal variability of the winds caused by diurnal sea breezes [e.g., *Woodson et al*., 2009]. Similar to the 3 week period, these upwelling (relaxation) cycles drive offshore cooling (warming) of the water column (Figure 8b). These cycles also generally result in shoaling (deepening) of the offshore thermocline and a decrease (increase) in the offshore internal wave activity, as seen in the phase speeds obtained from the normal mode analysis (Figures 8b and 8d, respectively). Furthermore, Figure 8c highlights the nearshore response of temperature and DO to the low-frequency winds and offshore stratification. That is, a general decrease (increase) in DO and temperature during upwelling (relaxation) periods. Moreover, there are numerous low oxygen (i.e., below 4.6 mg/L; hypoxic) events observed during upwelling periods over the 2.5 month record (Figure 8c).

A coherence analysis was performed on the upwelling favorable winds and the offshore thermocline depth over the 2.5 month record. The significant coherence at low frequencies (Figure 10) corroborates the fact that the offshore temperature structure is largely governed by wind-driven upwelling/relaxation cycles. Also evident in the coherence is a significant peak at the diurnal frequency, suggesting that the diurnal sea breeze also modulates the thermocline. While this diurnal frequency component was largely absent from the thermocline depth spectrum during the 3 week period, wavelet analysis (not shown) supports the fact that there is significant temporal variability in the diurnal frequency component of the offshore thermocline depth that is linked to periods of increased wind forcing.

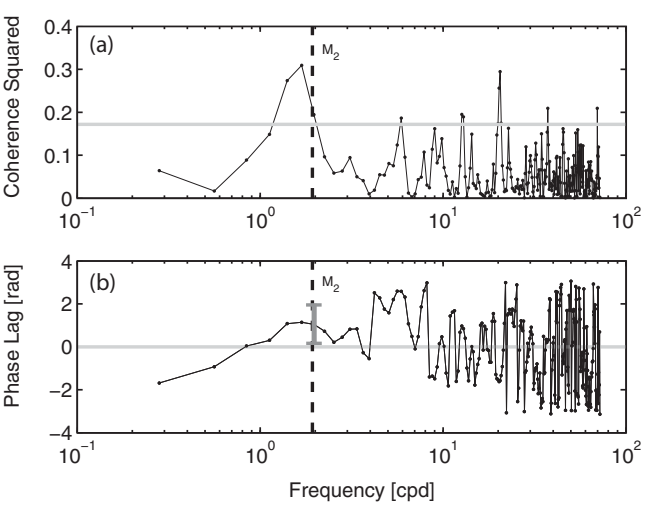

Figure 7. (a) Coherence squared and (b) phase lag between the high-pass filtered potential energy density anomaly (bore strength proxy) and the offshore thermocline depth (11.2°C isotherm) over the 3 week study period. The 90% confidence level is shown as a gray line in Figure 7a. The location of the M_2 tidal component is denoted by a dashed black line in Figures 7a and 7b. Confidence levels for the phase lag at the semidiurnal frequency (M_2 tidal component) are shown in Figure 7b as a gray error bar. A positive phase lag at a given frequency indicates that the bore strength proxy lags the offshore thermocline depth.

Figure 11 confirms that changes in the offshore stratification result in modification of the offshore internal wavefield. Specifically, increases (decreases) in the offshore thermocline depth generally result in increases (decreases) in the offshore normal mode phase speed, and therefore the strength of the offshore internal waves. In order to connect the offshore internal wave activity to nearshore internal bore activity, it is necessary to derive a new nearshore bore index over the 2.5 month record using the near-bottom temperature since the previously defined bore index (i.e., high-pass potential energy density anomaly) requires high-resolution vertical density measurements that are only available during the 3 week period. Figure 12a shows a scatter plot over the 3 week period of the windowed-standard deviation (1 day windows with 50% overlap;

© 2014. American Geophysical Union. All Rights Reserved.

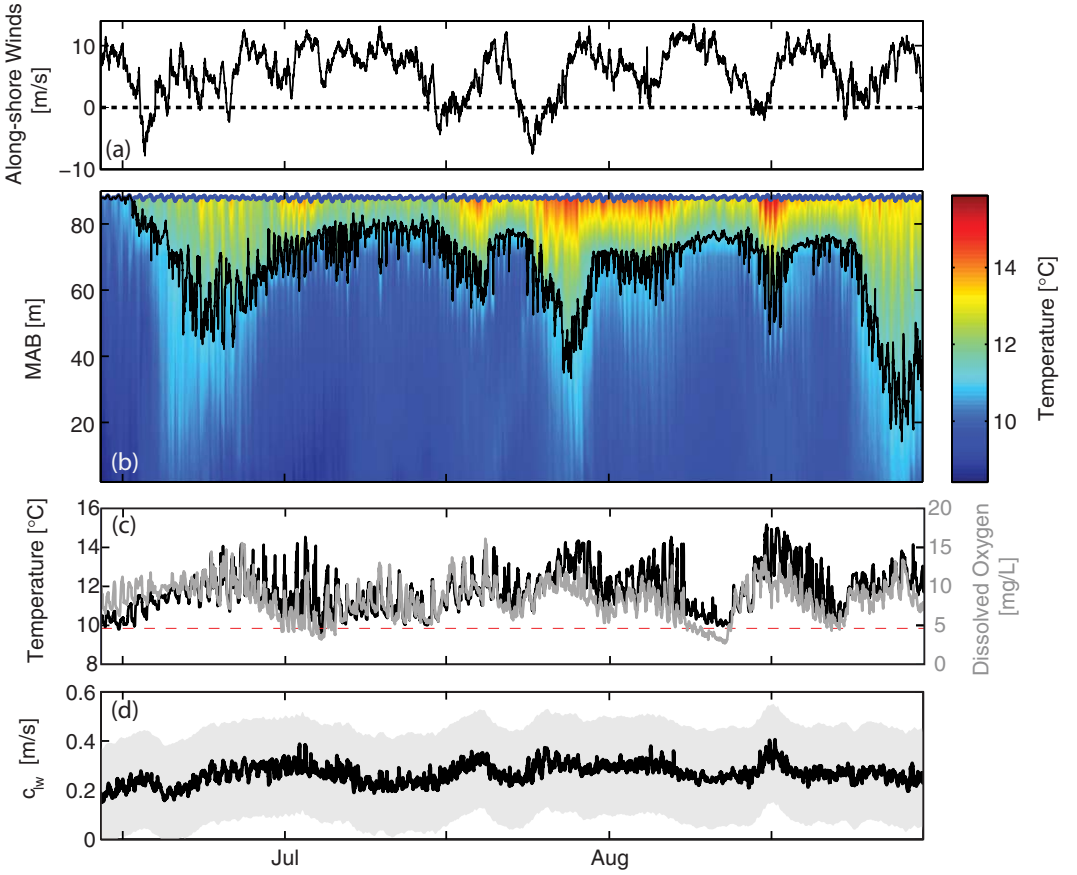

Figure 8. Time series over the ~2.5 month study period of the (a) regional upwelling favorable winds (positive), (b) vertical temperature structure at the offshore (OS) mooring (11.2°C isotherm shown as a solid black line to highlight the thermocline structure), (c) near-bottom temperature (left axis, black) and dissolved oxygen (right axis, gray) at the NS mooring, and (d) linear, longwave speeds from the OS mooring (black line) calculated using the OS stratification (10 min averages) and a normal mode analysis (section 2.3). The location of the sea surface (blue line) is shown in Figure 8b. The dashed red line in Figure 8c denotes the DO concentration identified by *Vaquer-Sunyer and Duarte* [2008] as a critical biological threshold (i.e., below 4.6 mg/L; hypoxic). The gray shading in Figure 8d denotes the phase speed in the presence of a typical barotropic current on the shelf of ±0.2 m/s [e.g., *Breaker and Broenkow*, 1994].

results not sensitive to choice of window used) of the near-bottom temperature versus the potential energy density anomaly bore strength index. The two quantities are highly correlated ($R^2 = 0.98$ for the bin-averaged values, p-value < 0.001), indicating that the standard deviation of the near-bottom temperature can be used as a proxy for nearshore internal bore activity. Figure 12b shows a scatter plot over the 2.5 month period of this nearshore bore proxy (standard deviation of the near-bottom temperature) versus the

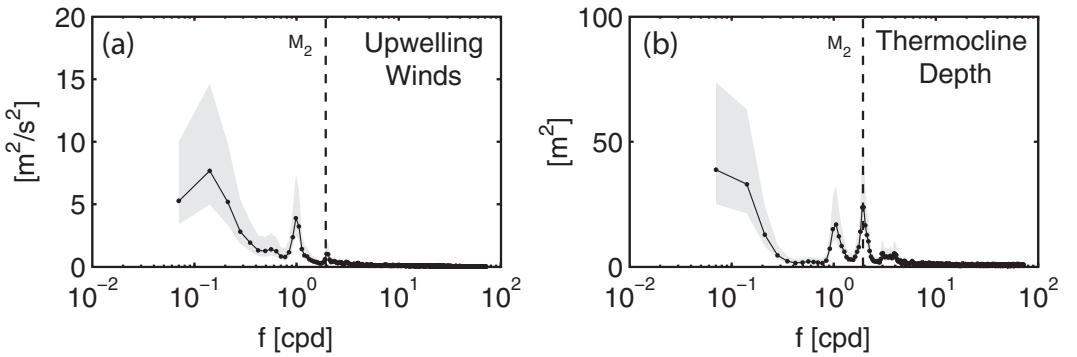

Figure 9. Variance-preserving power spectra over the ~2.5 month study period of the (a) regional upwelling winds and the (b) offshore thermocline depth (11.2°C isotherm). 80% confidence intervals are denoted by gray shading and the location of the M_2 tidal component by a dashed black line.

© 2014. American Geophysical Union. All Rights Reserved.

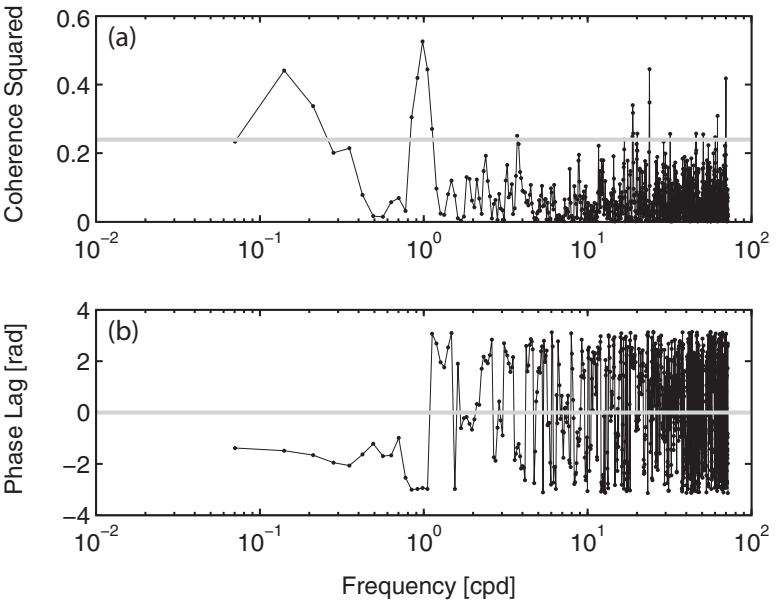

Figure 10. (a) Coherence squared and (b) phase lag between the regional upwelling favorable winds and the offshore thermocline depth (11.2°C isotherm) over the ~2.5 month study period. The 95% confidence level is shown as a gray line in Figure 10a. A negative phase lag at a given frequency indicates that the upwelling winds lead the offshore thermocline depth.

offshore internal wave activity (normal mode phase speeds), and highlights how increases (decreases) in the offshore internal wavefield translate into increases (decreases) in the nearshore bore field.

The results presented above offer insight into the connection between offshore and nearshore internal dynamics. We surmise that the internal bores observed in the nearshore are related to the onshore translation and propagation of the offshore internal tidal field (M_2 tidal component). However, it is important to note that there are other factors that complicate the dynamics and predictability of not only the nearshore internal bores, but also the transformation and propagation of the offshore internal wavefield to the nearshore [cf. *Nash et al.*, 2012]. The recent review by *Lamb* [2013], and the references therein [e.g., *Nash et al.*, 2012], provides a comprehensive overview of factors affecting the propagation and transformation of internal waves over the continental shelf. This includes, but is not limited to, strong barotropic tidal forcing, baroclinic effects and strong background shear, mesoscale and submesoscale variability, and complicated bathymetry including submarine canyons, all of which are found in the Monterey Bay region [*Breaker and Broenkow*, 1994].

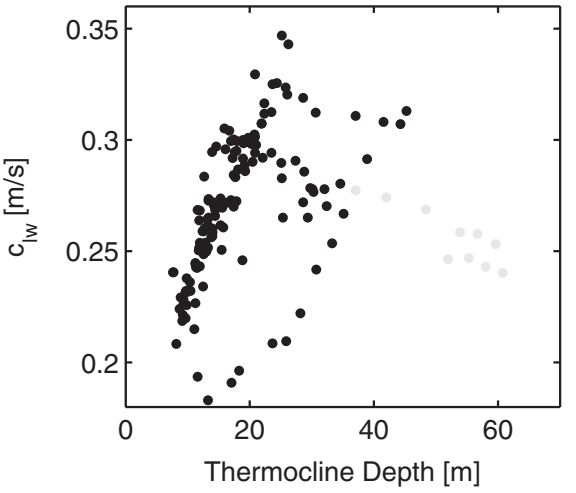

Figure 11. Scatterplot over the ~ 2.5 month study period of the windowed-mean linear, longwave speeds from the offshore (OS) mooring calculated using the OS stratification (10 min averages) and a normal mode analysis (section 2.3; proxy for the strength of the offshore internal wave/tide field) and the windowed mean of the OS thermocline depth (11.2°C isotherm). Mean values were calculated using 1 day windows with 50% overlap, and results were not sensitive to the choice of window used. The gray dots denote the period from 26 to 30 August, during which an extended relaxation event resulted in anomalously large thermocline depths.

There has also been considerable research into factors affecting the M_2 internal tide field in the Monterey Bay region, including the effects of the Monterey Submarine Canyon and Big Sur Ridge [e.g., *Carter*, 2010; *Kang and Fringer*, 2012]. However, the aforementioned studies are large-scale

© 2014. American Geophysical Union. All Rights Reserved.

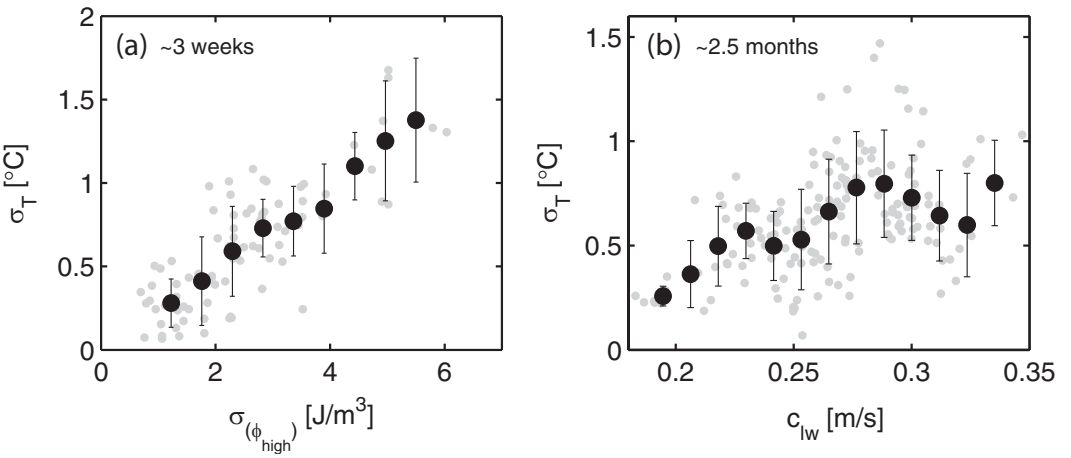

Figure 12. (a) Scatterplot over the 3 week study period of the windowed-standard deviation of the near-bottom temperature (long-term bore strength proxy) and the windowed-standard deviation of the high-pass filtered potential energy density anomaly (short-term bore strength proxy), both from the nearshore (NS) mooring. (b) Scatterplot over the 2.5 month study period of the windowed-standard deviation of the near-bottom temperature (long-term bore strength proxy) at the NS mooring and the linear, longwave speeds from the offshore (OS) mooring calculated using the OS stratification (10 min averages) and a normal mode analysis (section 2.3; proxy for the strength of the offshore internal wave/tide field). Windowed-standard deviation values were calculated using 1 day windows with 50% overlap, and results were not sensitive to the choice of window used. The gray dots denote the windowed values, while the black dots represent bin-averaged values. The black error bars on the bin-averaged values signify the standard deviation of the binned results.

modeling efforts that do not account for upwelling/relaxation cycles or variable environmental conditions (i.e., stratification) on the shelf, and do not accurately capture internal dynamics on the shelf and in the nearshore. It is also possible that the internal wavefield represents energy from multiple source locations (both locally and remotely generated internal tides), further complicating the predictability of the internal tide [cf. *Kelly and Nash*, 2010; *Nash et al*., 2012]. These factors make the predictability of the bores in the nearshore (and offshore) difficult, and might also explain why *Walter et al*. [2012] found no relationship between the arrival times of the nearshore bores and the phase of the local tides over a 2 week period. Future field and modeling studies are needed to assess the spatiotemporal variability of the internal tide field in Monterey Bay and elsewhere.

4.2. Oxygen Variability and Low Oxygen Events in the Nearshore

While it is well established that seasonal upwelling cycles contribute to oxygen variability and low oxygen events in the shallow waters along the eastern Pacific, the role of other physical processes is poorly understood [*Chan et al*., 2008]. In particular, previous observations near the study site clearly show regular intrusions of low DO water that are attributed to internal motions [*Booth et al*., 2012]. We expand on this work below and examine how nearshore internal bores in different upwelling regimes can lead to drastically different durations and onset rates of hypoxia in the nearshore.

Figures 13a and 13b show scatter plots over the 2.5 month study period of the windowed-standard deviation (1 day windows with 50% overlap; results not sensitive to choice of window used) of the near-bottom DO concentration versus the near-bottom temperature (i.e., long-term nearshore bore proxy). The important point is that there is extensive DO variability that is tightly linked to nearshore temperature variability (i.e., internal bore activity). Interestingly, the windowed-mean DO concentrations, seen as colored and scaled circles in Figure 13a, demonstrate that the lowest mean concentrations are observed during periods of reduced bore activity and oxygen variability. This coincides with periods of prolonged upwelling and nearshore pooling, whereby low oxygen waters (i.e., below 4.6 mg/L; hypoxic) are able to persist for several days. In contrast, Figure 13b shows the windowed-minimum DO concentrations and highlights that strong bore variability produces transient pulses of low oxygen (i.e., below 4.6 mg/L; hypoxic). This indicates that while extended upwelling periods with reduced bore activity are important for the duration of low DO events, individual bores can drive shock-like drops in DO with rapid onset times. Indeed, both onset time and duration of the low DO events are important for assessing potential impacts of hypoxia, each with likely different implications for nearshore ecological communities.

© 2014. American Geophysical Union. All Rights Reserved.

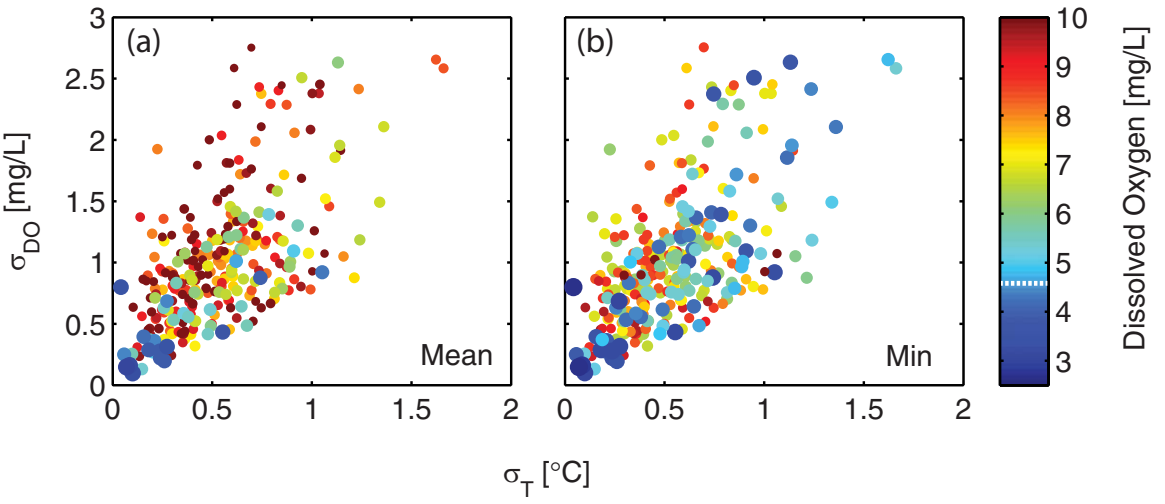

Figure 13. Scatterplot over the 2.5 month study period of the windowed-standard deviation of the near-bottom dissolved oxygen (DO) concentration and the windowed-standard deviation of the near-bottom temperature (long-term bore strength proxy), both from the nearshore (NS) mooring. Windowed-standard deviation values were calculated using 1 day windows with 50% overlap, and results were not sensitive to the choice of window used. The colored circles in Figures 13a and 13b denote the windowed-mean and windowed-minimum dissolved oxygen concentrations, respectively, as indicated in the colorbar. The size of the circles has also been scaled to highlight the low DO values (i.e., larger circles indicate lower DO concentrations). The dashed white line on the colorbar signifies the DO concentration identified by *Vaquer-Sunyer and Duarte* [2008] as a critical biological threshold (i.e., below 4.6 mg/L; hypoxic).

Monterey Bay, as part of the California Current Large Marine Ecosystem (CCLME), is listed as a "hotspot" for ecological risk from upwelled hypoxia [*Hofmann et al.*, 2011]. While the hypoxic durations presented here are relatively short (longest event lasts 3 days from 9 to 12 August), the high-frequency nature of individual bore events represent shock-like drops in oxygen which may amplify ecological impacts [*Burton et al.*, 1980]. Additionally, rockfish (*Sebastes* spp.), which are abundant at the study site, have shown profound response to DO concentrations slightly below the concentrations reported here [*Grantham et al.*, 2004]. Avoidance, which often occurs in reported ranges of 2–4 mg/L [*Wannamaker and Rice*, 2000; *Brady and Targett*, 2010], can drive much greater indirect impacts, through density-dependent factors, than direct lethal effects [*Eby and Crowder*, 2002; *Breitburg et al.*, 2009; *Craig*, 2012]. Furthermore, measurements reported here cover habitat for ecologically and commercially important species. Dungeness crabs (*Cancer magister*) and market squid (*Loligo opalescens*), two of California's most valuable commercial species, have shown major sensitivity to hypoxia [*Vojkovich*, 1998; *Grantham et al.*, 2004; *Zeidberg et al.*, 2006], and are particularly relevant here due to their dependence on habitat within this study site and their likely sensitivity to nearshore pooling [*Young et al.*, 2011; *Zeidberg et al.*, 2012].

4.3. Bores as a Mechanism for Cross-Shelf Exchange

Figure 14 shows vertical profiles of temperature and cross-shore velocity for a representative bore event on 16 August. The arrival of the bore and the dense, offshore waters are characterized by a strongly sheared baroclinic flow with onshore flow near the bed and offshore flow in the upper portion of the water column (Figure 14b). Eventually, the bore reverses direction and propagates back downslope with offshore flow near the bed and onshore flow near the surface. During this phase, the strongest cross-shelf velocities are observed, and the vertical profiles are bottom intensified (i.e., strongest near the bed). The flow reversal, or the relaxation of the bore back downslope, has been implicated in the onshore transport of larvae in the warm-water front that appears in Figure 14a (8:30–9:00) [e.g., *Pineda*, 1994] ("mixing period" in *Walter et al.* [2012]). We note that the Monterey Bay study site contains steeper bathymetric slopes and a more complex shoreline compared to the gradually sloping bathymetry typically found in Southern California [e.g., *Pineda*, 1994; *Wong et al.*, 2012] resulting in slightly different bore dynamics [see *Walter et al.*, 2012]. Nonetheless, this period of the bore event consistently has the strongest cross-shelf velocities, and previous observations indicate that elevated levels of diapycnal mixing in the stratified interior are observed during the warm-water relaxations [*Walter et al.*, 2012]. Thus, not only are scalars exchanged in the cross-shelf direction during these flows, but they are also likely mixed vertically.

We employed an empirical orthogonal function (EOF) analysis on the cross-shelf velocity field over the 3 week period to decompose the signal into its principal components, or dominant statistical modes. The EOF analysis

© 2014. American Geophysical Union. All Rights Reserved.

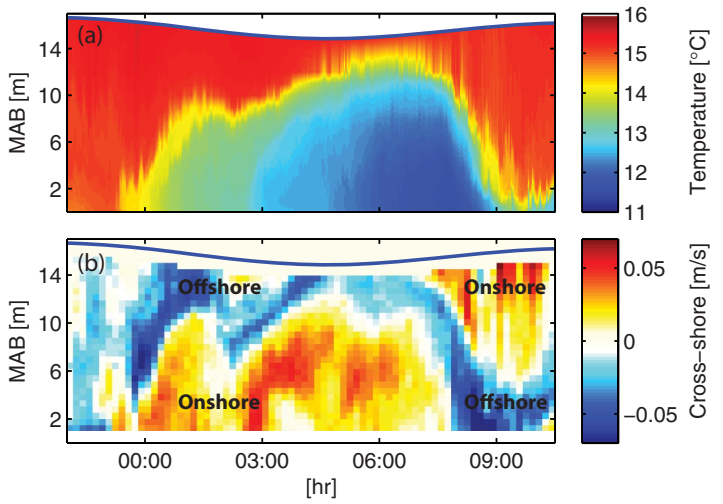

Figure 14. Example nearshore internal bore event from 16 August 2012. (a) Vertical temperature structure. (b) Cross-shore velocity structure (positive onshore, 10 min averages). The location of the sea surface (blue line) is shown in Figures 14a and 14b.

provides a description of the spatial variability of the velocity field through the modal shapes (eigenfunctions), as well as the temporally variability through the modal amplitude time series [*Emery and Thompson*, 2004]. Figure 15 highlights the vertical structure of the first three principal components (EOF modal shapes) of the cross-shore velocity field, along with the percent contribution of each mode to the total variance. The first mode, which describes 52.5% of the total variance, follows the vertical structure of the cross-shore velocity observed during the bore events (Figures 15 and 14b, respectively). Particularly, the profile represents a sheared baroclinic structure that is bottom intensified (i.e., nonzero depth average and largest magnitude near the bottom of the water column), similar to the bore events observed. Spectral analysis of the first mode amplitude time series reveals a dominant peak at the semidiurnal frequency (M_2 tidal component, Figure 4d). Furthermore, the coherence between the bore strength index and the first mode amplitude time series is significant at the semidiurnal frequency (M_2 tidal component, significant squared coherence of 0.52, not shown). This finding further supports the claim that the bores dominate cross-shelf exchange and transport in the nearshore, and that these bores likely contribute to the majority of the cross-shelf velocity variance observed. While velocity measurements were only available over the 3 week study period, long-term measurements in the region demonstrate that wind- and wave-driven cross-shelf exchange is small compared to exchange by internal bores [*Woodson*, 2013].

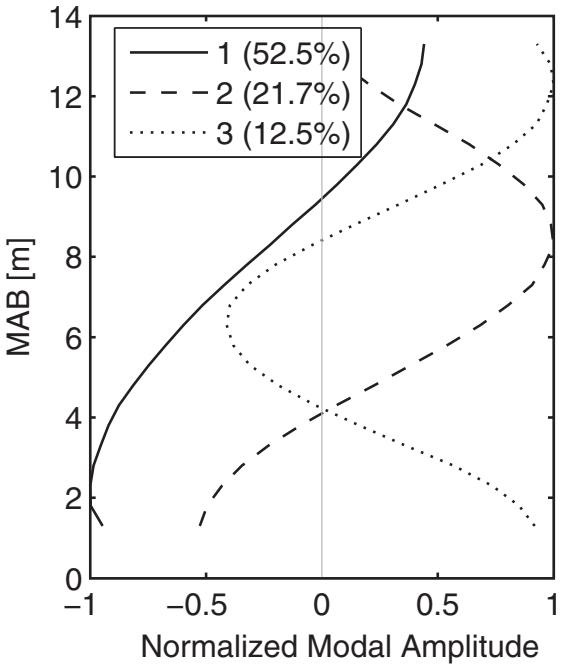

Figure 15. Vertical profiles for the first three statistical modes obtained from the EOF analysis for the cross-shore velocities over the 3 week study period. The first, second, and third modes are represented by solid, dashed, and dotted black lines, respectively, and the percent contribution to the total variance of each mode is also shown in the legend. The modal amplitude is normalized by the maximum vertical value for each component.

5. Summary

The ultimate fate of NLIWs and bores in shallow, nearshore regions (20 m) has been mainly speculative [cf. *Lamb* 2013], despite their biological and ecological implications [*Wolanski and Pickard*, 1983;

© 2014. American Geophysical Union. All Rights Reserved.

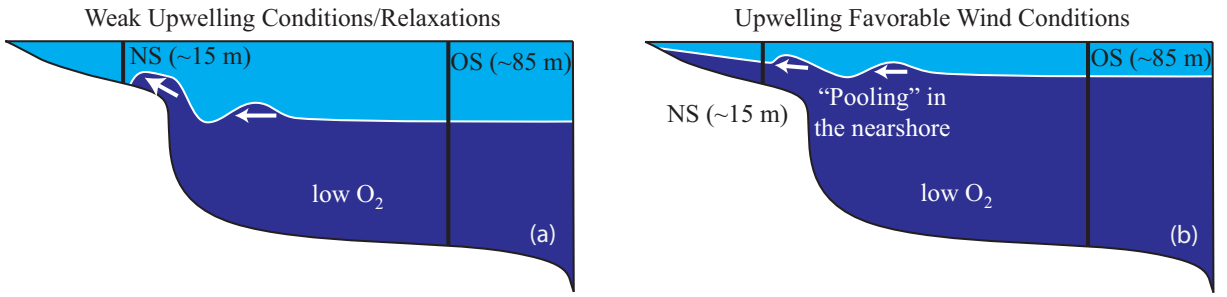

Figure 16. Schematic cartoon highlighting how wind-driven upwelling and offshore stratification influence nearshore internal bores. (a) During weak upwelling conditions/relaxations, the offshore thermocline is deeper, internal wave activity increases in the offshore, nearshore bore activity increases, and the bores propagate into well-mixed waters in the nearshore. (b) During upwelling favorable conditions, the offshore thermocline shoals toward the surface, offshore internal wave and nearshore bore activity both decrease, "pooling" develops in the nearshore, and the nearshore bores perturb a preexisting stratification.

Leichter et al., 1996; *Boehm et al.*, 2002; *Pineda*, 1991, 1994, 1995, 1999; *Booth et al.*, 2012; *Walter et al.*, 2012; *Wong et al.*, 2012]. *Pineda and Lopez* [2002] first hypothesized that low-frequency phenomena modulate the offshore stratification, and in turn affect nearshore internal bores in Southern California. We expand on this early work and present observations suggesting that low-frequency upwelling wind patterns modulate the offshore stratification and thermocline depth in southern Monterey Bay, CA, which in turn alters the strength and structure of the bores in the shallow, nearshore region (Figure 16).

The internal bore events are shown to contribute to the majority of the variance in cross-shelf exchange and transport in the nearshore. Furthermore, we link the nearshore oxygen variability to the nearshore bore activity. We show that individual bores can create short-lived low DO (hypoxic) events with shock-like onset times, but that extended upwelling periods are important for the duration of low DO episodes. Further assessment of how the strong DO variability and low DO (hypoxic) events affect nearshore communities is the subject of ongoing research. Likewise, future studies are needed to further assess the spatiotemporal variability of the internal wave/tide field in Monterey Bay [e.g., *Nash et al.*, 2012], including further assessment of its formation and energetics [*Carter*, 2010; *Kang and Fringer*, 2012]. We recognize that the detailed measurements throughout the water column at the nearshore site were only available over a 3 week study period, and that inferences were made about the nearshore internal bore field over the 2.5 month period using the near-bottom temperature (see section 4.1, Figure 12a). Given this, we stress that care should be taken in drawing generalized conclusions about the processes described, especially over longer time periods. Finally, the observations were collected during the late upwelling season in Monterey Bay; further observations are needed to assess the influence of the seasonal variability in the upwelling winds [cf. *García-Reyes and Largier*, 2012], and the oceanic response, as well as the extension of the results to other upwelling systems and sites.

Acknowledgments

This work was funded by the National Science Foundation through grants OCE-1235552 and DEB-1212124, and by the Singapore Stanford Program. R. Walter was supported by the Stanford Graduate Fellowship. This manuscript greatly benefited from the helpful comments of three anonymous reviewers. We acknowledge helpful discussions with Jeff Koseff, Derek Fong, Oliver Fringer, Kurt Rosenberger, Curt Storlazzi, and Olivia Cheriton. Data used in this study are available by contacting R. Walter. Offshore data used in this study were provided to R. Walter by the United States Geological Survey's Pacific Coastal and Marine Science Center. Bathymetry data used in this study were acquired, processed, archived, and distributed by the Seafloor Mapping Lab of California State University Monterey Bay.

References

Alford, M. H., J. B. Mickett, S. Zhang, P. MacCready, Z. Zhao, and J. Newton (2012), Internal waves on the Washington continental shelf, *Oceanography*, *25*(2), 66–79, doi:10.5670/oceanog.2012.43.

Bakun, A. (1990), Global climate change and intensification of coastal ocean upwelling, *Science*, *247*(4939), 198–201, doi:10.1126/science.247.4939.198.

Beardsley, R. C., C. E. Dorman, C. A. Friehe, L. K. Rosenfeld, and C. D. Winant (1987), Local atmospheric forcing during the coastal ocean dynamics experiment: 1. A description of the marine boundary layer and atmospheric conditions over a northern California upwelling region, *J. Geophys. Res.*, *92*, 1467–1488.

Boegman, L., G. N. Ivey, and J. Imberger (2005), The degeneration of internal waves in lakes with sloping topography, *Limnol. Oceanogr. Methods*, *50*, 1620–1637, doi:10.4319/lo.2005.50.5.1620.

Boehm, A. B., B. F. Sanders, and C. D. Winant (2002), Cross-Shelf transport at Huntington Beach: Implications for the fate of sewage discharged through an offshore ocean outfall, *Environ. Sci. Technol.*, *36*, 1899–1906.

Bograd, S. J., C. G. Castro, E. Di Lorenzo, D. M. Palacios, H. Bailey, W. Gilly, and F. P. Chavez (2008), Oxygen declines and the shoaling of the hypoxic boundary in the California Current, *Geophys. Res. Lett.*, *35*, L12607, doi:10.1029/2008GL034185.

Booth, J. A. T., et al. (2012), Natural intrusions of hypoxic, low pH water into nearshore marine environments on the California coast, *Cont. Shelf Res.*, *45*, 108–115.

Brady, D. C., and T. E. Targett (2010), Characterizing the escape response of juvenile summer flounder Paralichthys dentatus to diel-cycling hypoxia, *J. Fish Biol.*, *77*(1), 137–52, doi:10.1111/j.1095-8649.2010.02663.x.

Breaker, L. C., and W. W. Broenkow (1994), The circulation of Monterey Bay and related processes, *Oceanogr. Mar. Biol.*, *32*, 1–64.

Breitburg, D. L., D. W. Hondorp, L. A. Davias, and R. J. Diaz (2009), Hypoxia, nitrogen, and fisheries: Integrating effects across local and global landscapes, *Annu. Rev. Mar. Sci.*, *1*, 329–349, doi:10.1146/annurev.marine.010908.163754.

© 2014. American Geophysical Union. All Rights Reserved.

Burton, D. T., L. B. Richardson, and C. J. Moore (1980), Effect of oxygen reduction rate and constant low dissolved oxygen concentrations on two estuarine Fish, *Trans. Am. Fish. Soc.*, *559*, 552–557.
Carter, G. S. (2010), Barotropic and baroclinic M_2 tides in the Monterey Bay region, *J. Phys. Oceanogr.*, *40*, 1766–1783.
Chan, F., J. A. Barth, J. Lubchenco, A. Kirincich, H. Weeks, W. T. Peterson, and B. A. Menge (2008), Emergence of anoxia in the California Current large marine ecosystem, *Science*, *319*, 920–920.
Colosi, J. A., R. C. Beardsley, J. F. Lynch, G. Gawarkiewicz, C. Chiu, and A. Scotti (2001), Observations of nonlinear internal waves on the outer New England continental shelf during the summer Shelfbreak Primer study, *J. Geophys. Res.*, *106*, 9587–9601.
Craig, J. K. (2012), Aggregation on the edge: Effects of hypoxia avoidance on the spatial distribution of brown shrimp and demersal fishes in the Northern Gulf of Mexico, *Mar. Ecol. Prog. Ser.*, *445*, 75–95, doi:10.3354/meps09437.
Davis, K. A., and S. G. Monismith (2011), The modification of bottom boundary layer turbulence and mixing by internal waves shoaling on a barrier reef, *J. Phys. Oceanogr.*, *41*, 2223–2241.
Eby, L. A., and L. B. Crowder (2002), Hypoxia-based habitat compression in the Neuse River Estuary: Context-dependent shifts in behavorial avoidance thresholds, *Can. J. Fish. Aquat. Sci.*, *59*, 952–965.
Ekau, W., H. Auel, H.-O. Pörtner, and D. Gilbert (2010), Impacts of hypoxia on the structure and processes in pelagic communities (zooplankton, macro-invertebrates and fish), *Biogeosciences*, *7*(5), 1669–1699, doi:10.5194/bg-7-1669-2010.
Emery, W. J., and R. E. Thomson (2004), *Data Analysis Methods in Physical Oceanography*, 2nd revised ed., 638 pp., Elsevier, Amsterdam.
Frieder, C. A., S. H. Nam, T. R. Martz, and L. A. Levin (2012), High temporal and spatial variability of dissolved oxygen and pH in a nearshore California kelp forest, *Biogeosciences*, *9*(10), 3917–3930, doi:10.5194/bg-9-3917-2012.
García-Reyes, M., and J. L. Largier (2012), Seasonality of coastal upwelling off central and northern California: New insights, including temporal and spatial variability, *J. Geophys. Res.*, *117*, C03028, doi:10.1029/2011JC007629.
Grantham, B. A., F. Chan, K. J. Nielsen, D. S. Fox, J. A. Barth, A. Huyer, J. Lubchencho, and B. A. Menge (2004), Upwelling-driven nearshore hypoxia signals ecosystem and oceanographic changes, *Nature*, *429*, 749–754, doi:10.1038/nature02612.1.
Helly, J. J., and L. A. Levin (2004), Global distribution of naturally occurring marine hypoxia on continental margins, *Deep Sea Res., Part I*, *51*(9), 1159–1168, doi:10.1016/j.dsr.2004.03.009.
Hofmann, A. F., E. T. Peltzer, P. M. Walz, and P. G. Brewer (2011), Hypoxia by degrees: Establishing definitions for a changing ocean, *Deep Sea Res., Part I*, *58*(12), 1212–1226.
Holloway, P. E. (1987), Internal hydraulic jumps and solitons at a shelf break region on the Austrialian NorthWest Shelf, *J. Geophys. Res.*, *92*, 5405–5416.
Hosegood, P., and H. van Haren (2004), Near-bed solibores over the continental slope in the Faeroe-Shetland Channel, *Deep Sea Res., Part II*, *51*, 2943–2971.
Kamykowski, D., and S. Zentara (1990), Hypoxia in the world ocean as recorded in the historical data set, *Deep Sea Res., Part A*, *37*(12), 1861–1874.
Kang, D., and O. B. Fringer (2010), On the calculation of available potential energy in internal wave fields, *J. Phys. Oceanogr.*, *40*, 2539–2545, doi:10.1175/2010JPO4497.1.
Keeling, R. F., and H. E. Garcia (2002), The change in oceanic O_2 inventory associated with recent global warming, *Proc. Natl. Acad. Sci. U. S. A.*, *99*(12), 7848–7853, doi:10.1073/pnas.122154899.
Kelly, S. M., and J. D. Nash (2010), Internal-tide generation and destruction by shoaling internal tides, *Geophys. Res. Lett.*, *37*, L23611, doi:10.1029/2010GL045598.
Kildow, J., and C. S. Colgan (2005), California's Ocean Economy, Report to the Resources Agency, State of California, report, pp. 1–156, Natl. Ocean Econ. Program, Monterey, Calif.
Klymak, J. M., and J. N. Moum (2003), Internal solitary waves of elevation advancing on a shoaling shelf, *Geophys. Res. Lett.*, *30*(20), 2045, doi:10.1029/2003GL017706.
Kunze, E., L. K. Rosenfeld, G. S. Carter, and M. C. Gregg (2002), Internal waves in Monterey Submarine Canyon, *J. Phys. Oceanogr.*, *32*, 1890–1913.
Lamb, K. G. (2013), Internal wave breaking and dissipation mechanisms on the continental slope/shelf, *Annu. Rev. Fluid Mech.*, *46*, 231–254.
Leichter, J. J., S. R. Wing, S. L. Miller, and M. W. Denny (1996), Pulsed delivery of subthermocline water to Conch Reef (Florida Keys) by internal tidal bores, *Limnol. Oceanogr.*, *41*, 1490–1501.
Lerczak, J. A., C. D. Winant, and M. C. Hendershott (2003), Observations of the semidiurnal internal tide on the southern California slope and shelf, *J. Geophys. Res.*, *108*(C3), 3068, doi:10.1029/2001JC001128.
Mann, K. H. (2000), *Ecology of Coastal Waters, With Implications for Management*, 406 pp., Blackwell Sci., Oxford, U. K.
McClatchie, S., R. Goericke, R. Cosgrove, G. Auad, and R. Vetter (2010), Oxygen in the Southern California Bight: Multidecadal trends and implications for demersal fisheries, *Geophys. Res. Lett.*, *37*, L19602, doi:10.1029/2010GL044497.
Nam, S., and U. Send (2011), Direct evidence of deep water intrusions onto the continental shelf via surging internal tides, *J. Geophys. Res.*, *116*, C05004, doi:10.1029/2010JC006692.
Nash, J. D., M. H. Alford, and E. Kunze (2005), Estimating internal wave energy fluxes in the ocean, *J. Atmos. Oceanic Technol.*, *22*, 1551–1570.
Nash, J. D., E. L. Shroyer, S. M. Kelly, M. E. Inall, T. F. Duda, M. D. Levine, N. L. Jones, and R. C. Musgrave (2012), Are any coastal internal tides predictable?, *Oceanography*, *25*(2), 80–95.
Noble, M., B. Jones, P. Hamilton, J. Xu, G. Robertson, L. Rosenfeld, and J. Largier (2009), Cross-shelf transport into nearshore waters due to shoaling internal tides in San Pedro Bay, CA, *Cont. Shelf Res.*, *29*, 1768–1785.
Pauly, D., and V. Christensen (1995), Primary production required to sustain global fisheries, *Nature*, *374*, 255–257.
Petruncio, E. T., L. K. Rosenfeld, and J. D. Paduan (1998), Observations of the internal tide in Monterey Canyon, *J. Phys. Oceanogr.*, *28*, 1873–1903.
Pineda, J. (1991), Predictable upwelling and the shoreward transport of planktonic larvae by internal tidal bores, *Science*, *253*, 548–549.
Pineda, J. (1994), Internal tidal bores in the nearshore: Warm-water fronts, seaward gravity currents and the onshore transport of neustonic larvae, *J. Mar. Res.*, *52*, 427–458.
Pineda, J. (1995), An internal tidal bore regime at nearshore stations along western USA: Predictable upwelling within the lunar cycle, *Cont. Shelf Res.*, *15*(8), 1023–1041.
Pineda, J. (1999), Circulation and larval distribution in internal tidal bore warm fronts, *Limnol. Oceanogr.*, *44*, 1400–1414.
Pineda, J., and M. Lopez (2002), Temperature, stratification, and barnacle larval settlement in two Californian sites, *Cont. Shelf Res.*, *22*, 1183–1198.
Raheem, N., et al. (2012), Application of non-market valuation to California's coastal policy decisions, *Mar. Policy*, *36*, 1–6.

© 2014. American Geophysical Union. All Rights Reserved.

Rosenfeld, L. K., F. B. Schwing, N. Garfield, and D. E. Tracy (1994), Bifurcated flow from an upwelling center: A cold water source for Monterey Bay, *Cont. Shelf Res.*, *14*, 931–964.
Rosenfeld, L. K., I. Shulman, M. Cook, J. D. Paduan, and L. Shulman (2009), Methodology for regional tidal model evaluation, with application to Central California, *Deep Sea Res., Part II*, *56*, 199–218.
Sandstrom, H., and J. A. Ellitot (1984), Internal tide and solitons on the Scotian Shelf: A nutrient pump at work, *J. Geophys. Res.*, *89*, 6415–6426.
Scotti, A., and J. Pineda (2004), Observation of very large and steep internal waves of elevation near the Massachusetts coast, *Geophys. Res. Lett.*, *31*, L22307, doi:10.1029/2004GL021052.
Shea, R. E., and W. W. Broenkow (1982), The role of internal tides in the nutrient enrichment of Monterey Bay, California, *Estuarine Coastal Shelf Sci.*, *15*, 57–66.
Shroyer, E. L., J. N. Moum, and J. D. Nash (2009), Observations of polarity reversal in shoaling nonlinear internal waves, *J. Phys. Oceanogr.*, *39*, 691–701.
Simpson, J. H., C. M. Allen, and N. C. G. Morris (1978), Fronts on the continental shelf, *J. Geophys. Res.*, *83*, 4607–4614, doi:10.1029/JC083iC09p04607.
Stramma, L., G. C. Johnson, J. Sprintall, and V. Mohrholz (2008), Expanding oxygen-minimum zones in the tropical oceans, *Science*, *320*(5876), 655–658, doi:10.1126/science.1153847.
Stramma, L., S. Schmidtko, L. A. Levin, and G. C. Johnson (2010), Ocean oxygen minima expansions and their biological impacts, *Deep Sea Res., Part I*, *57*(4), 587–595, doi:10.1016/j.dsr.2010.01.005.
Vaquer-Sunyer, R., and C. M. Duarte (2008), Thresholds of hypoxia for marine biodiversity, *Proc. Natl. Acad. Sci. U.S.A.*, *105*, 15,452–15,457.
Venayagamoorthy, S. K., and O. B. Fringer (2007), On the formation and propagation of nonlinear internal boluses across a shelf break, *J. Fluid Mech.*, *577*, 137.
Vojkovich, M. (1998), The California fishery for market squid (Loligo opalescens), *CalCOF Invest. Rep. 39*, pp. 55–60, CalCOFI, La Jolla, CA.
Walter, R. K., N. J. Nidieko, and S. G. Monismith (2011), Similarity scaling of turbulence spectra and cospectra in a shallow tidal flow, *J. Geophys. Res.*, *116*, C10019, doi:10.1029/2011JC007144.
Walter, R. K., C. B. Woodson, R. S. Arthur, O. B. Fringer, and S. G. Monismith (2012), Nearshore internal bores and turbulent mixing in southern Monterey Bay, *J. Geophys. Res.*, *177*, C07017, doi:10.1029/2012JC008115.
Wannamaker, C., and J. Rice (2000), Effects of hypoxia on movements and behavior of selected estuarine organisms from the southeastern United States, *J. Exp. Mar. Biol. Ecol.*, *249*(2), 145–163.
Wolanski, E., and G. Pickard (1983), Upwelling by internal tides and Kelvin waves at the continental shelf break on the Great Barrier Reef, *Aust. J. Mar. Freshwater Res.*, *34*, 65–80.
Wong, S. H. C., A. E. Santoro, N. J. Nidzieko, J. L. Hench, and A. B. Boehm (2012), Coupled physical, chemical, and microbiological measurements suggest a connection between internal waves and surf zone water quality in the Southern California Bight, *Cont. Shelf Res.*, *34*, 64–78.
Woodson, C. B. (2013), Spatiotemporal variation in cross-shelf exchange across the inner shelf of Monterey Bay, CA, *J. Phys. Oceanogr.*, *43*, 1648–1665.
Woodson, C. B., L. Washburn, J. A. Barth, D. J. Hoover, A. R. Kirincich, M. A. McManus, J. P. Ryan, and J. Tyburczy (2009), Northern Monterey Bay upwelling shadow front: Observations of a coastally and surface-trapped buoyant plume, *J. Geophys. Res.*, *114*, C12013, doi:10.1029/2009JC005623.
Woodson, C. B., et al. (2011), Observations of internal wave packets propagating along-shelf in northern Monterey Bay, *Geophys. Res. Lett.*, *38*, L01605, doi:10.1029/2010GL045453.
Wyrtki, K. (1962), The oxygen minima in relation to ocean circulation, *Deep Sea Res. Oceanogr. Abstr.*, *9*(1–2), 11–23, doi:10.1016/0011-7471(62)90243-7.
Young, M. A., R. G. Kvitek, P. J. Iampietro, C. D. Garza, R. Maillet, and R. T. Hanlon (2011), Sea floor mapping and landscape ecology analyses used to monitor variations in spawning site preference and benthic egg mop abundance for the California market squid (*Doryteuthis opalescens*), *J. Exp. Mar. Biol. Ecol.*, *407*(2), 226–233, doi:10.1016/j.jembe.2011.06.017.
Zeidberg, L. D., W. M. Hamner, N. Nezlin, and A. Henry (2006), The fishery for California market squid (*Loligo opalescens*) (Cephalopoda: Myopsida), from 1981 through 2003, *Fish. Bull.*, *104*(1), 46–59.
Zeidberg, L. D., J. L. Butler, D. Ramon, A. Cossio, K. L. Stierhoff, and A. Henry (2012), Estimation of spawning habitats of market squid (*Doryteuthis opalescens*) from field surveys of eggs off Central and Southern California, *Mar. Ecol.*, *33*(3), 326–336, doi:10.1111/j.1439-0485.2011.00498.x.

© 2014. American Geophysical Union. All Rights Reserved.